

Shallow granular flows

Daisuke Takagi, Jim N. McElwaine, and Herbert E. Huppert

Department of Applied Mathematics and Theoretical Physics, Institute of Theoretical Geophysics, Centre for Mathematical Sciences, University of Cambridge, Wilberforce Road, Cambridge CB3 0WA, United Kingdom

(Received 28 October 2009; revised manuscript received 16 December 2010; published 24 March 2011)

Many processes in geophysical and industrial settings involve the flow of granular materials down a slope. In order to investigate the granular dynamics, we report a series of laboratory experiments conducted by releasing grains at a steady rate from a localized source on a rough inclined plane. Different types of dense granular flow are observed by varying the flow rate at the source and the slope of the inclined plane. The two cases of steady flow confined by levees and the flow of avalanches down the plane are examined. The width of the steady flow increases linearly with the prescribed flow rate, which does not appreciably affect the characteristic depth or surface velocity of the bulk flow. When the flow rate is just below that required for sustaining the steady flow, avalanches are triggered at regular intervals. The avalanches maintain their shape, size, and speed down the inclined plane. We propose a simple model of steady flow that is consistent with our observations and discuss the challenges associated with the theoretical treatment of avalanche dynamics.

DOI: [10.1103/PhysRevE.83.031306](https://doi.org/10.1103/PhysRevE.83.031306)

PACS number(s): 45.70.-n, 47.57.Gc, 47.57.Qk

I. INTRODUCTION

Numerous natural hazards involve the flow of granular materials on mountainous terrain. Examples include debris flows [1], rockfalls, and snow avalanches [2]. These natural flows have the potential to destroy everything along their path; and, therefore, they are a serious danger to life and infrastructure on mountains. A continuous stream often develops into a succession of waves of higher speeds and masses, which can be particularly destructive. In order to conduct hazard analysis and to protect inhabited areas, for example, by diverting the descending waves with barriers [3,4], the size and speed of the waves must be predicted. Related problems arise in agricultural, manufacturing, and pharmaceutical industries. Fertilizers, metal parts, and medical pills are examples of grains that are managed and are transported in large quantities. A quantitative understanding of dense granular flows [5,6] is helpful for predicting natural flows and engineering industrial processes. However, our understanding of granular flows is far from complete, particularly in shallow layers where flowing and static regions can simultaneously exist.

Laboratory experiments have shed some light on shallow granular flows of cohesionless grains. An avalanche triggered on a horizontal plane [7,8], a curved slope [9–11], or an erodible granular layer on a rough inclined plane [12] causes grains in a shallow layer to flow during a short interval from initiation to termination. A series of avalanches can be triggered intermittently by releasing grains at a small and steady rate down a gentle slope [13–15]. On steeper slopes, longitudinal [16,17] and transverse [18] instabilities develop on the flowing surface and produce avalanches down the plane. A steady flow of granular material is sustained by releasing grains at a sufficiently large rate down a rough plane inclined at a range of intermediate angles [16,19–22].

An empirical law for the steady flow down the plane has been derived from a series of experiments and simulations [5,13,20,21]. The law is given by

$$\frac{U}{\sqrt{gh}} = \alpha + \beta \frac{h}{h_{\text{stop}}}, \quad (1)$$

where U is the depth-averaged velocity, h is the flow depth, h_{stop} is the thickness of the layer that naturally deposits on the incline when the flow stops, g is gravitational acceleration, and α and β are dimensionless parameters. However, Eq. (1) and other theories [23–25] do not accurately describe how shallow layers with thickness close to h_{stop} can be either static or flowing. Open problems remain in addressing nonlocal effects that play a role in shallow layers close to jamming [26–28], a phenomenon exhibited similarly by yield stress fluids [29,30]. Shallow granular flows must be better understood in order to conduct hazard analysis by predicting paths of natural flows, which are often close in thickness to h_{stop} as they spread out over an open slope [13,31–33].

The dynamics of granular layers with thickness close to h_{stop} can be examined in the laboratory by releasing grains from a localized source on a rough inclined plane. Previous experiments showed that spherical beads of diameter 0.35 ± 0.05 mm, released steadily on a rough incline, develop a thin flowing layer with nearly static margins [13]. Further experiments showed that the flow gradually becomes thinner and wider in time [32]. The authors of this paper claim that the structure of the flow approaches a steady state. However, we conducted similar experiments, but for longer periods, by releasing spherical beads of the same diameter at a rate of 4.6–21.0 g/s on rough slopes of 24° – 26° and discovered that the margins of the flow eventually become unstable, leading to considerable spatiotemporal variations in the flowing structure after a typical time of 70–90 min. Steady flow does not become unstable when the beads are replaced with the more generic material of nonspherical grains of sand, as reported here, indicating that the shape of grains plays an important role in shallow granular flows. The possible reasons for the difference in behavior of different grains are discussed in Sec. IV. In Sec. II, we describe how grains are supplied at a steady rate from a localized source on a rough inclined plane in the laboratory. In Sec. III, the results are presented in three parts. The first part provides an overview of the new types of granular flows of sand that arise by varying the flow rate and the slope of the inclined plane. The second part examines the steady flow

confined by levees at different flow rates. Effects of the shape of the grains and any erodible grains on the plane before initiating the flow are presented. The third part examines how the steady release of sand at a rate that is just below that required for sustaining the steady flow results in the flow of avalanches triggered at regular intervals. Our preliminary study of steady flows and regular avalanches, observed on a plane inclined at intermediate angles, provides a foundation for future studies of intermittent avalanches [34] and roll waves [16], which develop on gentler and steeper slopes, respectively.

II. METHOD

We carried out a series of laboratory experiments to investigate the flow of dry grains from a localized source on a rough inclined plane. The experimental setup is shown in Fig. 1. A cylindrical, perspex hopper of diameter 250 mm and height 700 mm was filled with granular material. Two different granular materials were used; spherical glass beads of diameter 0.35 ± 0.05 mm or nonspherical sand grains of size 0.45 ± 0.15 mm. Experiments were conducted primarily with sand rather than glass beads because the latter introduced additional complications, as reported below. The bottom of the hopper was connected to a cone that fed the grains into a smooth pipe of diameter 30 mm. A control valve across

the pipe allowed the mass flow rate Q to be set to 0 or controlled between 5 and 218 g s^{-1} , with a repeatability better than $\pm 2 \text{ g s}^{-1}$ for sand. Below the control valve, the grains fell freely down a tube onto a block of foam, which was highly inelastic and absorbed the energy of the impacting grains on the inclined plane. There was a V-shaped groove cut into the middle of the foam to produce a localized source of dense granular flow.

The grains flowed down an inclined plane of length 3 m and width 1 m, wider than any of the flows in the experiments. The plane was made rough by gluing the same sand on the surface. Before each experimental run, the plane was covered in an erodible layer of uniform thickness h_{stop} , unless otherwise stated. This configuration allowed the system to approach any long-time state more quickly than an inclined plane initially free of grains, as reported below. The erodible layer was set up by releasing a large flux of grains and then abruptly stopping the flow, a technique adopted previously [20]. A pulley system allowed the plane to be inclined at any angle in the range between 0° and 45° to the horizontal with an accuracy of 0.1° , as measured by a digital inclinometer. The flows in the experiments could be maintained indefinitely by transferring the grains that flowed off the inclined plane back into the hopper.

The thickness and surface velocity of the flows were measured at different times and positions down the plane. Variations across steady flows, as reported in detail below, were examined as follows. The thickness profile was measured to an accuracy of ± 0.1 mm at 1000 Hz over a region of length ≈ 130 mm using a laser triangulator (Micro-Epsilon LLT2800–100 2D laser displacement measuring system). The instrument was mounted on a linear traverse system to verify that steady flows were uniform down the inclined plane. For steady flows with widths greater than 130 mm, the instrument was positioned to observe one edge rather than the whole flow. Surface velocities were measured to an accuracy of $\pm 0.3 \text{ mm s}^{-1}$ with a high-speed camera (Photron SA1 5400 fps, 1024×1024 pixels, 12-bit analog-to-digital converter) using particle image velocimetry [35]. The cross-stream thickness and velocity profiles of steady flows were averaged over 30 s to reduce statistical fluctuations. Effects due to the flow rate and the presence of any erodible grains on the plane before the experiment were investigated on a slope of 32° to the horizontal, which allowed steady flows to develop over approximately the widest range of flow rates.

Variations along avalanches were examined by recording the thickness along the centerline of the flow at a fixed position down the slope. The shape, size, and speed of an avalanche are computed from the thickness profiles at successive times that are translated steadily along the slope. The translation speed c and the mean thickness profile f are obtained by minimizing a measure of deviations of the translated profiles,

$$\sum_i \sum_j [h(x_i, t_j) - f(x_i - ct_j)]^2, \quad (2)$$

where h represents the thickness recorded at discrete positions x_i and times t_j . The speed corresponds to the wave speed of avalanches, based on the assumption that avalanches retain their shape and size as they travel steadily, as shown below. The

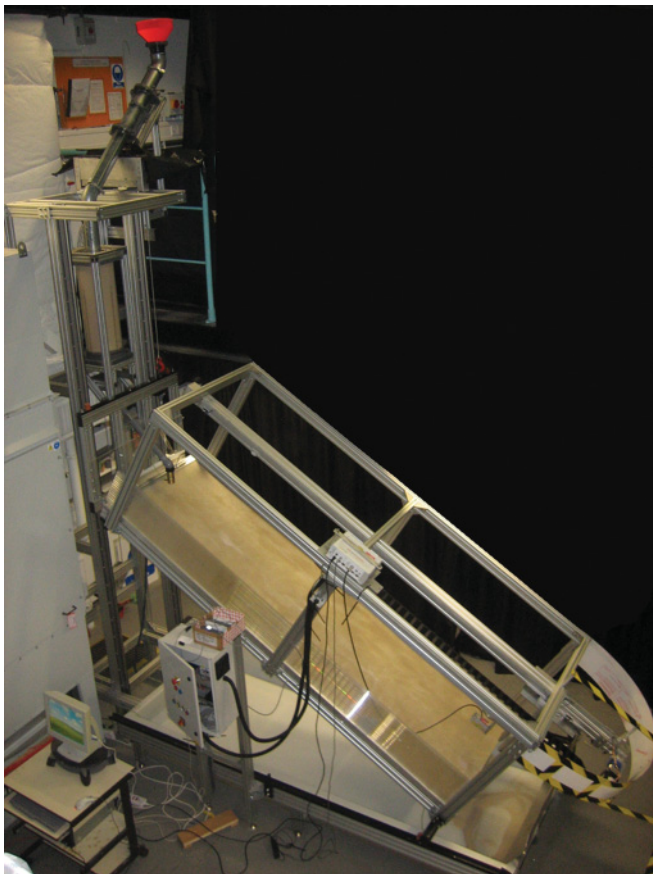


FIG. 1. (Color online) Photograph shows the experimental setup. The cylindrical hopper of sand, the rough inclined plane, and the instruments used to measure the flow are all supported by an aluminum framework.

computed speeds have been verified using images captured by the high-speed camera, which offers an alternative method of computing the speed of avalanches.

III. RESULTS

A. Overview

Different types of granular flows of sand develop depending on the angle of inclination of the rough plane and the mass flow rate. The different possible states of sand flow are marked in the regime diagram in Fig. 2, as studied in a similar fashion for glass beads [13]. The qualitative boundaries between the regimes are sketched in Fig. 3.

All the different regimes can be obtained by fixing the mass flow rate and varying only the slope of the inclined plane. On gentle slopes with θ less than 31° , avalanches are triggered intermittently on a heap of sand of ever-growing size. When θ lies between the range of 31° and 33° , either a series of avalanches or a steady stream propagates on a dense layer of erodible grains, depending on the flow rate. The avalanches can be triggered at regular intervals, as examined further below. When θ lies between approximately 33° and 38° , roll waves develop on the surface of dense granular flow [16], which can result in avalanches far downstream. Finally, on steeper slopes with θ greater than 38° , a dilute suspension of grains saltate down the plane [36].

Of particular interest in this paper is the intermediate range of angles between 31° and 33° . Within this range, there exists a minimum flow rate required for steady flow. When the supply of grains is turned off, the flow gradually stops and deposits a layer of thickness h_{stop} on the inclined plane. The thickness of the final deposited layer depends on the angle of inclination of the plane as shown in Fig. 4. The thickness for the moderate

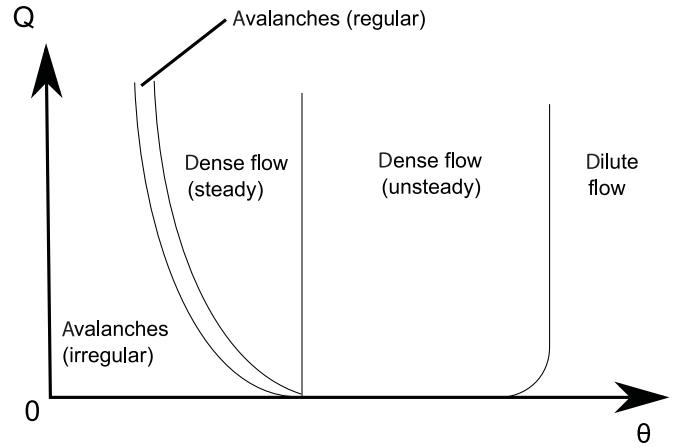


FIG. 3. A sketch of the salient regimes in Fig. 2. The regime of regular avalanches, as investigated here, marks the boundary between irregular avalanches and dense steady flow.

range of inclination angles, bounded by approximately 31° and 39° , is well described by a curve of the form [34]

$$\frac{h_{\text{stop}}}{d} = \frac{a}{\tan \theta - \tan \theta_1}, \quad (3)$$

where d is the particle diameter and $a = 0.48$ and $\theta_1 = 30.1^\circ$ are dimensionless parameters. A layer of thickness less than h_{stop} is unable to flow. We discuss later how h_{stop} , which characterizes the roughness and the slope of the inclined plane, appears in the condition for regular avalanches to develop.

In order to better understand the different regimes, we first examine the steady flow down a plane inclined at 32° . Effects on the steady flow due to the flow rate and any presence of erodible grains on the plane are investigated. We then examine how the steady release of sand at a rate, which is just below that required to sustain the steady flow, results in a series of avalanches triggered at regular intervals. The avalanches are shown to flow down the plane without changing shape, or speed.

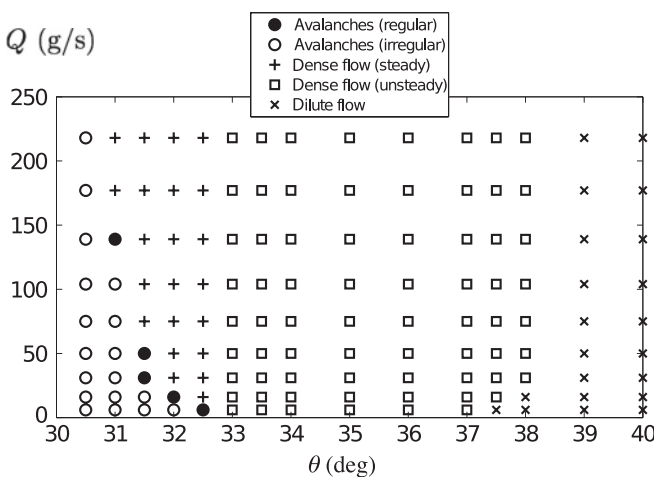


FIG. 2. Regime diagram showing the different types of sand flows as a result of a supply at a steady rate Q down a rough plane inclined at an angle θ to the horizontal. Avalanches are triggered at regular or irregular intervals down gentle slopes with $\theta < 33^\circ$ when the flow rate is small. At larger flow rates, dense granular flow develops and remains steady. On steeper slopes, the dense flow becomes unsteady downstream as roll waves develop.

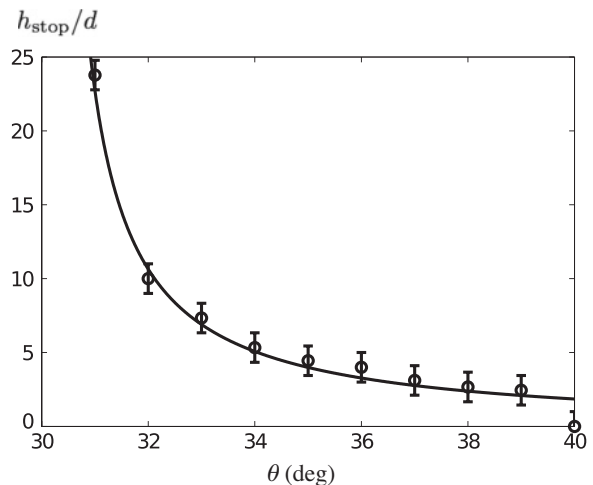


FIG. 4. The thickness of the deposit on the rough plane, scaled by the mean size of individual grains ($d \approx 0.45$ mm), as measured on the plane inclined at different angles. The line is given by Eq. (3) with $a = 0.48$ and $\theta_1 = 30.1^\circ$.

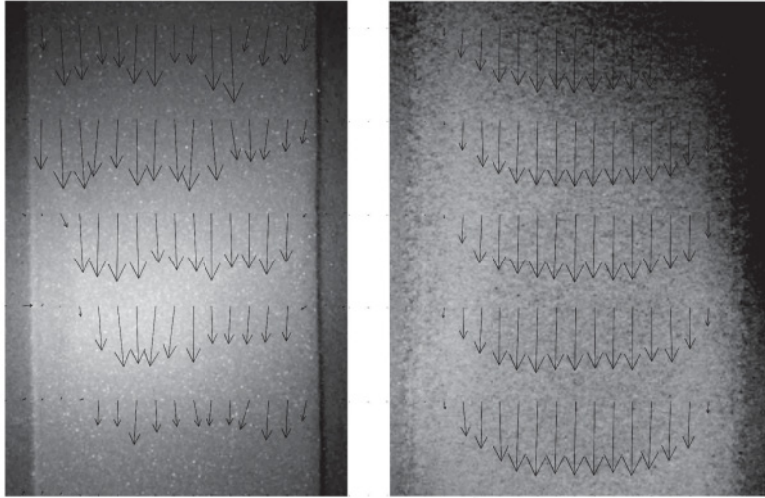
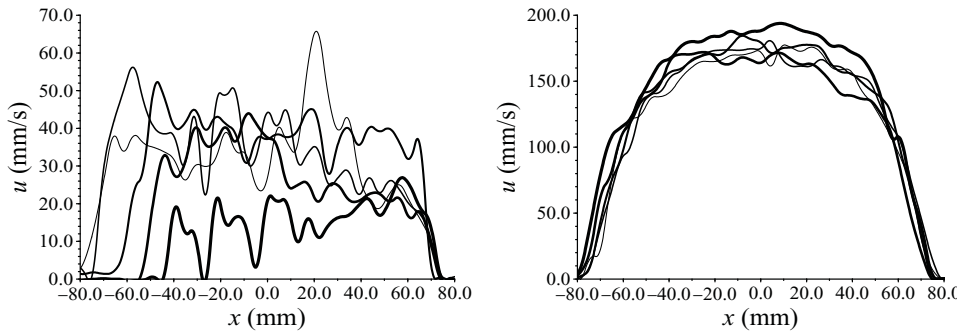


FIG. 5. Top left, plan form of beads and top right, sand flowing down a rough inclined plane. The snapshot was taken approximately 2 m down the plane, 90 min after initiating and sustaining a steady flow rate of beads at 10 g/s down a 25° slope or sand at 104 g/s down a 32° slope. The length of arrows, which originate at positions 10 mm apart in the cross-slope direction and 50 mm apart in the down-slope direction, represents the displacement of beads per second or that of sand per a fifth of a second. Five profiles at different extents downstream are plotted bottom left, for beads and bottom right, sand. The flow of beads is unsteady and that of sand is steady, as supported by the strong variations of the velocity in both the cross-stream and downstream directions for beads and negligible variations downstream for sand.



B. Steady flow

All experiments conducted using glass beads resulted in unsteady flow. A representative snapshot of the plan form and the instantaneous velocity profile of the flowing surface is shown in Fig. 5. At the margins, a region of no motion forms, grows, and propagates downstream. The downstream velocity along the centerline of the flow generally decreases with time while fluctuations in the velocity increase with time. A representative evolution of the mean and ten standard

deviations of the velocity along the centerline of the flow of beads are shown in Fig. 6. In contrast, a simpler system of steady flow could be observed using sand. The mean and fluctuations in surface velocity tend to constant values with time, as shown in Fig. 7 for a representative experiment conducted using sand. All experiments reported subsequently were conducted using sand.

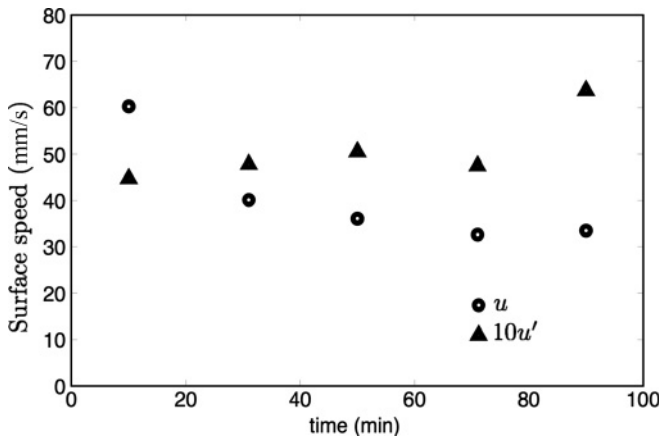


FIG. 6. Evolution of the mean (u) and ten standard deviations ($10u'$) of the surface velocity 2 m down a rough plane inclined at 25° to the horizontal where beads are released at a steady rate of 10 g/s. Fluctuations of the system grow with time.

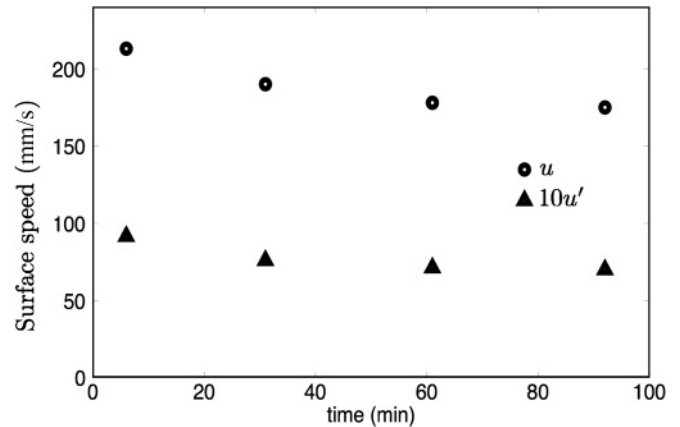


FIG. 7. Evolution of the mean (u) and ten standard deviations ($10u'$) of the surface velocity 2 m down a rough plane inclined at 32° to the horizontal where sand grains are released at a steady rate of 104 g/s. The system approaches a state with small fluctuations relative to the mean flow.

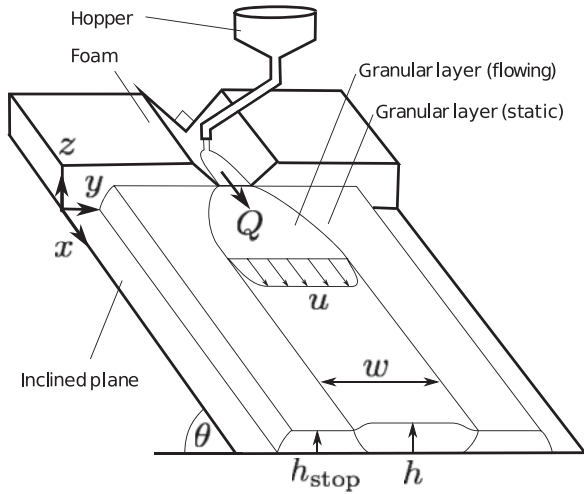


FIG. 8. Sketch of an experimental run producing a steady flow. Sand in the hopper is released onto the V-shaped foam and flows down the rough inclined plane. The bulk layer of the resultant flow has thickness h , width w , and surface velocity u , confined by static layers of sand of thickness h_{stop} . The angle of inclination of the plane $\theta = 32^\circ$ is fixed, and the steady mass flow rate Q is chosen within a wide range.

Our results show that steady flows of sand develop for mass flow rates ranging between 31 and 218 g s^{-1} down a plane inclined at 32° to the horizontal. A sketch of the flow is shown in Fig. 8. Steady flows are not sustainable at lower flow rates; instead, avalanches are triggered, as examined later.

Figure 9 shows the thickness and the surface velocity across the flow, sustained by releasing grains at a rate of $Q = 50 \text{ g s}^{-1}$ down a 32° slope initially free of grains. There is a gradual decrease in the height and the maximal velocity once the initial flow front has passed the measurement point. Note that the curves at 30 and 40 min in Fig. 9 overlay each other, indicating that the system has reached an approximately steady state. We verified, by conducting experiments for over 2 h, that both the thickness and the width of the flow tend to constant values with

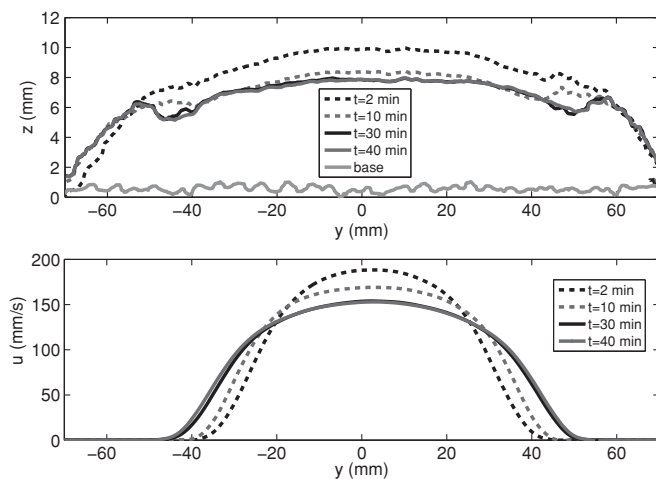


FIG. 9. Thickness and surface velocity of sand 2 m down a 32° slope, which is initially free of sand. Both the characteristic thickness and the surface velocity decrease slowly with time until a steady state is reached. The value of h_{stop} is 4.5 mm .

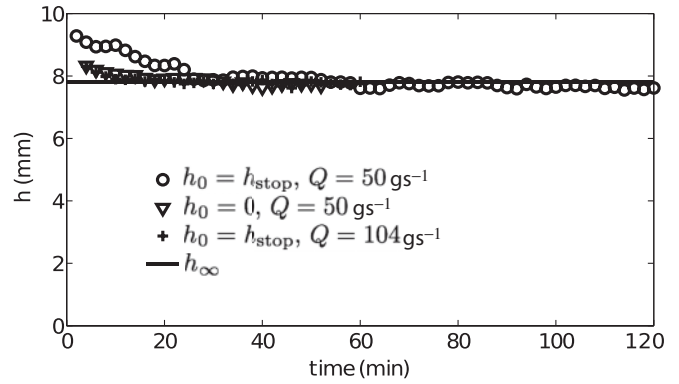


FIG. 10. Maximal thickness of sand is plotted against time for three representative experiments down a 32° slope. The inclined plane is either covered with an erodible layer of thickness h_{stop} ($h_0 = h_{stop}$) or free of sand initially ($h_0 = 0$), and the flow rate is sustained subsequently at either $Q = 50$ or 104 g s^{-1} . In all cases, the thickness approaches the same value, h_∞ .

time. A characterization of the convergence to steady state is given by Fig. 10, which shows the evolution of the maximal thickness.

Figure 11 shows the corresponding results of another run initiated differently by covering the incline to a thickness h_{stop} and maintaining the same flow rate as before. The flow attains a steady state more quickly, as indicated by the coinciding curves at 12 and 20 min. Figure 12 shows that the steady velocity profiles coincide with the previous case, indicating that the long-time steady state is independent of the initial conditions on the incline. Figure 10 shows that the maximal thickness of the flow approaches a constant value more quickly when the inclined plane is initially filled with an erodible layer of thickness h_{stop} . All the steady flows discussed subsequently in the paper were from experiments with the initial covering of grains to a thickness of h_{stop} .

Steady flows obtained at different flow rates all feature a central region of approximately constant thickness and a pair

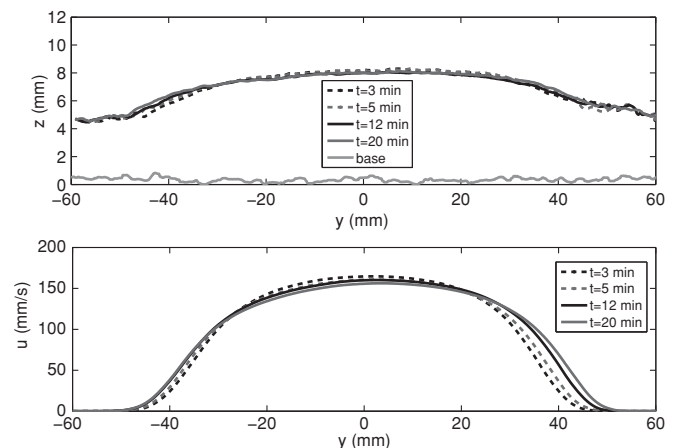


FIG. 11. Thickness and surface velocity of sand 2 m down a 32° slope initially covered with a static erodible layer of thickness $h_{stop} = 4.5 \text{ mm}$. Minimal variations with time indicate that the flow quickly reaches a steady state.

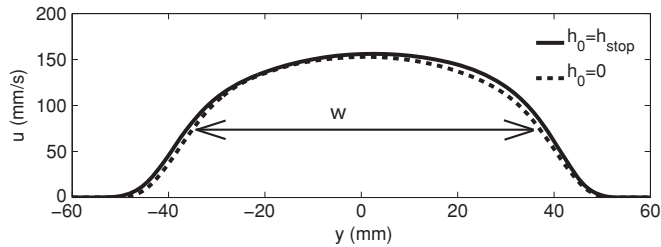


FIG. 12. Steady surface velocity profiles in the long-time limit on a 32° slope, covered initially with no sand ($h_0 = 0$) and with an erodible layer of sand ($h_0 = h_{\text{stop}}$). The mass flow rate is $Q = 50 \text{ g/s}$ in both experiments. The width of the region with surface velocity greater than half the maximal velocity is represented by w .

of margins where the thickness decreases to h_{stop} . The central region is characterized by its width w , maximal thickness h , and surface velocity attained at the center of the flow u . The width of the flow increases linearly with the mass flow rate as shown in Fig. 13, where w is defined as the width of the region with surface velocity greater than one half of its maximum attained at the center (cf. Fig. 12). This definition is a suitable measure with minimal noise because the ends of the region have large variations in velocity across the flow. We have considered other definitions of the width, including the width of the region of nonzero velocity [32], which changes the intercept w_0 but gives the same slope as shown by the approximately parallel lines of best fit in Fig. 13. The error bars are comparable to both the size of the symbols and the linear norms of residuals of the two fitting lines (12 to 13 mm). The width of the flow increases linearly with the flow rate at long times, such as at early times, as previously studied [13].

The thickness of the central flow is independent of the flow rate and shows no systematic deviation, as shown in Fig. 14. In contrast to the observations and theory of Ref. [32], the bulk region of the flowing layer in all our experiments is approximately flat in the transverse direction of the flow with a maximal thickness of $8.3 \pm 0.4 \text{ mm}$. The thickness is greater than, but the same order of magnitude as, $h_{\text{stop}} \approx 4.5 \text{ mm}$. The thickness is slightly greater than h_{stop} and independent of the flow rate, as in the thickness of the deposit formed by stopping the flow at early times [13].

The surface velocity increases weakly with the flow rate and appears to approach a finite limit as $Q \rightarrow \infty$, as shown

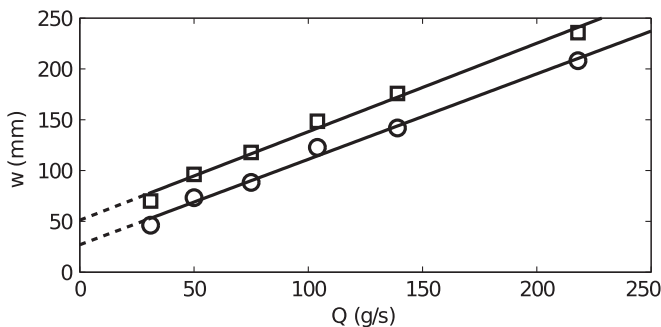


FIG. 13. Squares, characteristic width of the flowing region with nonzero velocity and circles, surface velocity greater than half the maximal velocity attained at the center of the flow plotted against the mass flow rate. Each line of best fit is extrapolated to $Q = 0$.

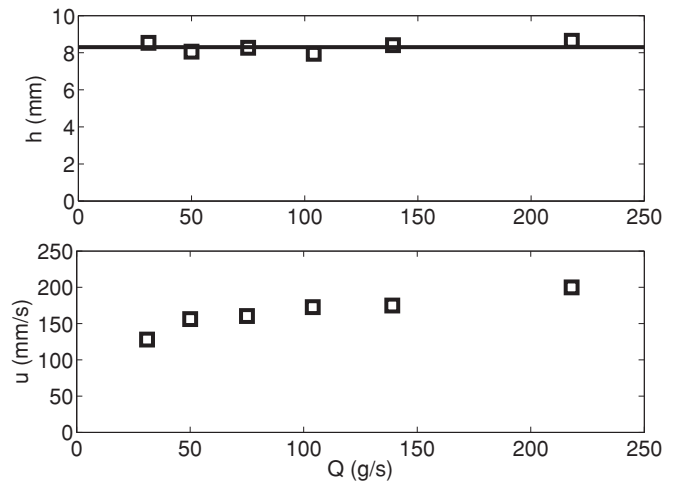


FIG. 14. Maximal thickness and surface velocity of steadily flowing sand as functions of the mass flow rate Q .

in Fig. 14. There is a relatively large change between $Q = 31$ and $Q = 50 \text{ g s}^{-1}$, but from here to $Q = 218 \text{ g s}^{-1}$, a 430% increase in mass flow rate, the velocity only increases from 158 to 200 mm s^{-1} , a 26% increase. The increase in velocity with increasing mass flow rate, without any change in the flow depth, is attributed to the reduced influence of lateral stresses as h/w decreases. The surface velocity varies strongly at the margins and weakly in the central region, suggesting that lateral stresses are most important at the margins but also play a role in the center of the flow even at a small aspect ratio of 1/20. Because of the lateral stresses, we cannot infer a linear relationship between the dimensionless speed and the dimensionless depth of the layer near one margin, which is shown in Fig. 15. Lateral variations in the surface velocity toward one margin of the flow for different flow rates are shown in Fig. 16. The approximate collapse of the velocity profiles suggests that the margins of the flowing layer are independent of the mass flow rate. Note that the length scale of the margins is comparable in order of magnitude to w_0 . It is not possible to sustain a steady flow below a certain flow rate as the flow width approaches w_0 .

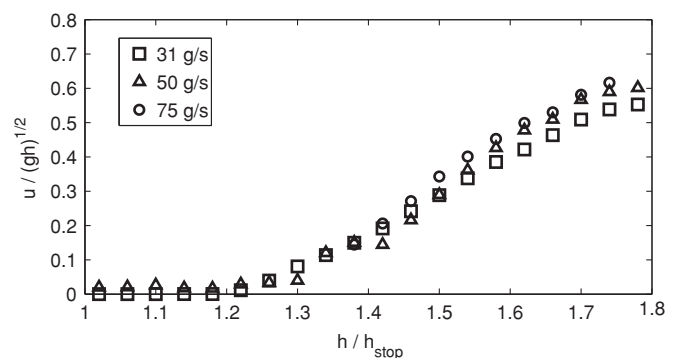


FIG. 15. Plot of the dimensionless speed against dimensionless height at the margins.

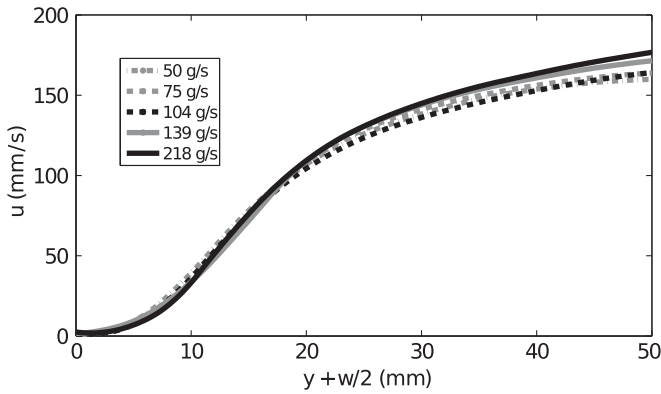


FIG. 16. Surface velocity profiles across the slope near one margin of the flowing layer for different mass flow rates.

C. Avalanches

When the flow rate is just below that required for steady flow, pulses of avalanches are triggered at approximately regular intervals. First, a relatively deep pile of sand grows near the source. After some time, an avalanche is triggered and propagates down the incline in a solitary wave. The avalanche leaves behind a layer of deposit at rest and erodes any static layer ahead of the front. The avalanche comes to a halt when there is no more erodible layer of sand ahead of the flow. In this manner, an erodible layer of static sand is produced and extends down the incline. Successive avalanches are triggered and propagate down the incline on the erodible layer, produced by the deposit of earlier avalanches. The avalanches remain stable and correspond to those in region II as plotted in Fig. 1(a) of Ref. [18].

The intervals in time between the arrival of successive avalanches can be computed readily by measuring the thickness of sand down the inclined plane. A representative set of results is presented for sand released at $Q = 16$ g/s down a 32° slope, which is initially free of grains. Figure 17 shows

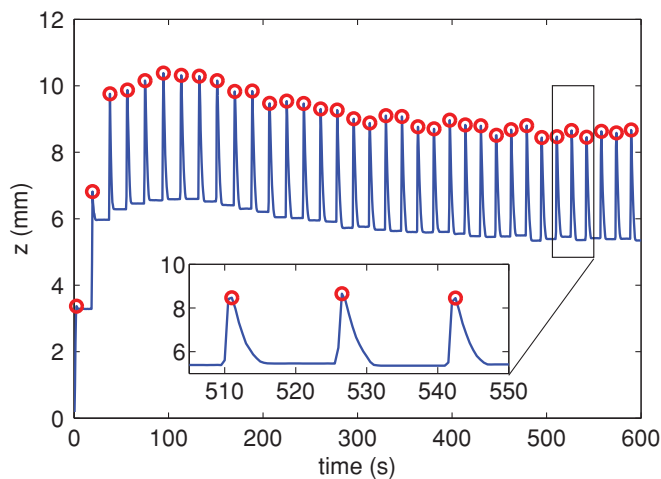


FIG. 17. (Color online) A plot of the mean thickness of the layer of sand 2 m down the incline from the source, averaged over half-second intervals near the beginning of an experiment with $Q = 16$ g/s and $\theta = 32^\circ$. Time begins from the moment when the first avalanche reaches the 2-m mark. The local maxima are represented by circles and correspond to the arrival of avalanches.

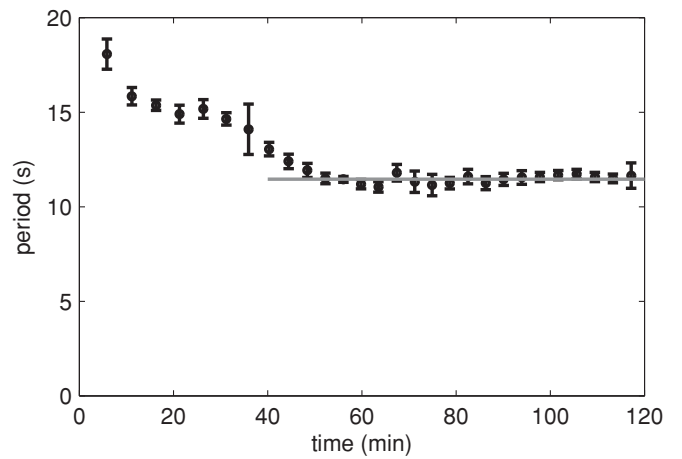


FIG. 18. The time interval between the arrival of successive avalanches plotted against time. Each data point is the mean period of 20 successive avalanches. The error bars show the standard deviation of the period of the same 20 avalanches. After approximately 50 min, the period remains close to 11.5 s, as marked by the horizontal line. This indicates that avalanches arrive at regular intervals in the long-time limit.

an evolution of the mean thickness of the layer of sand 2 m down the slope. The local maxima are represented by circles and correspond to the arrival of avalanches. The local minima correspond to the static layer that is deposited following the passage of avalanches. The mean and standard deviation of 20 intervals in time between the arrival of successive avalanches are shown in Fig. 18. The intervals decrease slowly with time until approximately 50 min into the experiment. The intervals remain close to 11.5 s, subsequently, indicating that avalanches arrive at regular intervals in the long-time limit. We noted that the approach to the long-time state is quicker when the plane is initially covered with an erodible layer of thickness h_{stop} . The subsequent analysis is based on experiments initiated on an inclined plane covered with erodible sand.

The regular interval between successive avalanches at large times increases on a gentler slope, which is associated with an

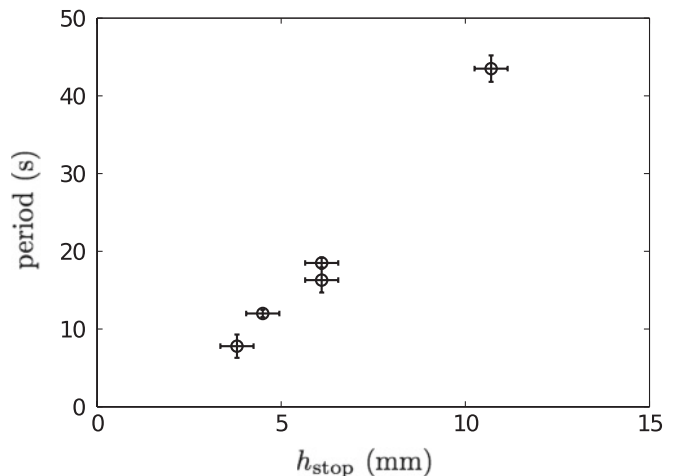


FIG. 19. Period of avalanches triggered at regular intervals increases with h_{stop} . This means that the interval between successive avalanches is longer down a more gentle slope.

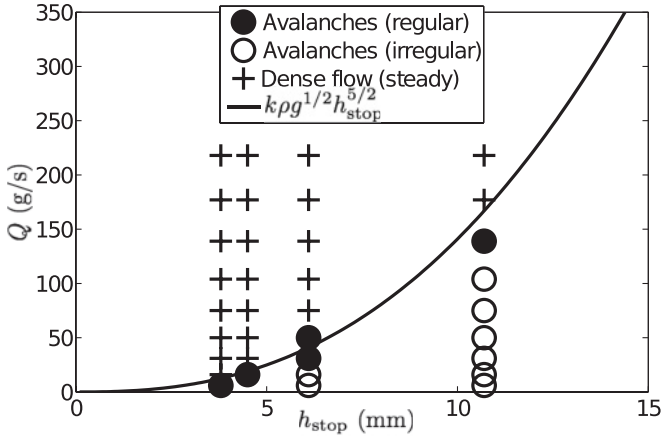


FIG. 20. The minimum flow rate required for steady flow is estimated by Eq. (7), where the constant of proportionality is $k \approx 3$.

increase in h_{stop} , as shown in Fig. 19. Moreover, an increase in h_{stop} increases the minimum flow rate required for steady flow as shown in Fig. 20. This means that the mass of grains in each avalanche, which is the product of the interval and the steady rate of supply at the source, increases sharply with h_{stop} . Avalanches initiated at regular intervals occur less frequently and are more massive on more gentle slopes.

The shape and size of avalanches are presented in the representative case of sand supplied at a rate of $Q = 16 \text{ g/s}$ down a 32° slope. The thickness profile of a representative avalanche 2 m down the slope is shown in Fig. 21. The thickness increases sharply at the front and decreases gently toward the back of the wave. The flow fluctuations are represented by one standard deviation above and below the mean curve. Thickness profiles of five successive avalanches were found to collapse with variations comparable to the flow fluctuations. This indicates that avalanches of similar shape and size travel down the slope. Figure 22 shows the thickness profile of representative avalanches at different extents down the slope. The profiles indicate that avalanches do not change

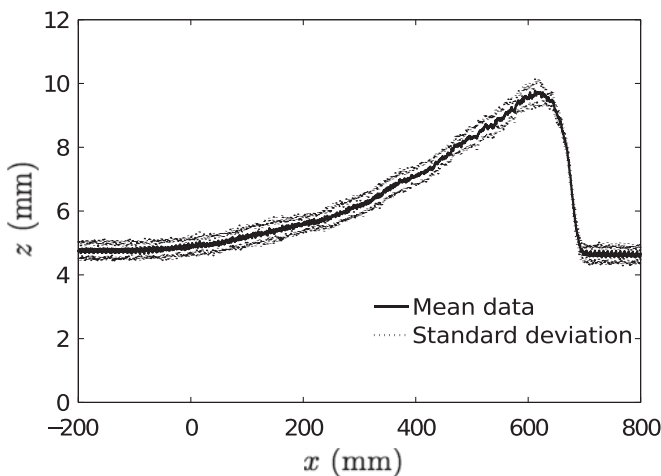


FIG. 21. The mean and standard deviation of the thickness profile of an avalanche 2 m down a 32° slope. Variations in the thickness profile of an avalanche due to flow fluctuations are small and are comparable with variations among successive avalanches.

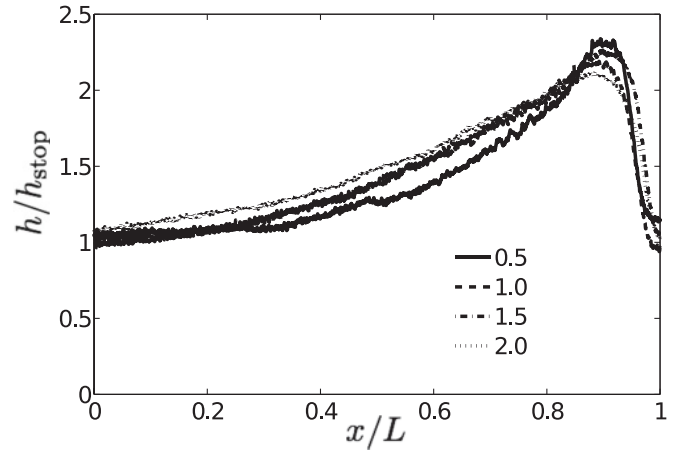


FIG. 22. Dimensional thickness profile of representative avalanches at 0.5, 1.0, 1.5, and 2.0 m down a 32° slope. The horizontal length is scaled by $L \approx 700 \text{ mm}$, and the vertical length is scaled by $h_{\text{stop}} \approx 4.5 \text{ mm}$. The mean profiles almost overlap, suggesting that avalanches retain their shape and size as they propagate downstream.

appreciably in shape or size as they travel down the slope. The speed of wave propagation is approximately constant as indicated by Fig. 23.

The dimensionless wave speed is plotted against the maximal thickness attained near the front of avalanches on different slopes in Fig. 24. The wave speed c is scaled by $\sqrt{gh_{\text{stop}} \cos \theta}$ and the maximal thickness h_f by h_{stop} . Avalanches initiated at regular intervals from a point source down different slopes with θ ranging between 31° and 32.5° , as investigated here, have approximately constant wave speed, $c = 0.6 \pm 0.1$. These avalanches are comparable in size and speed to those recorded in Fig. 2(b) of Ref. [18] but generally are slower in speed and are closer in thickness to h_{stop} than the avalanches triggered from a steady line source on steeper slopes with θ ranging between 32° and 41° [37].

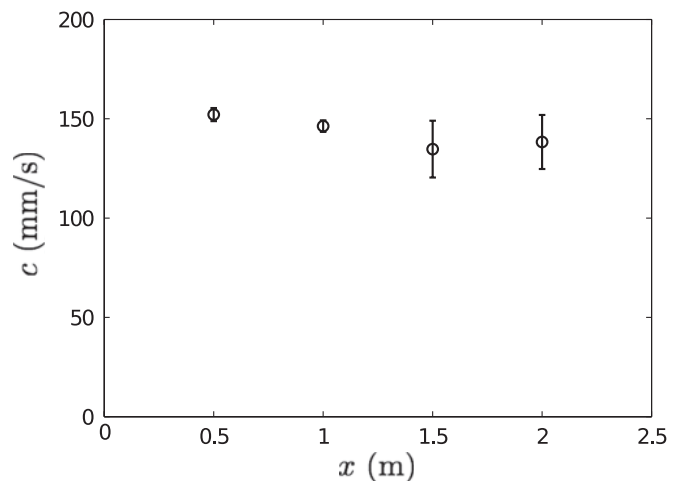


FIG. 23. Mean and standard deviation of the wave speed of ten representative avalanches at different extents down a 32° slope. The speed of each avalanche remains approximately constant during the course of its propagation. Variations in the wave speed are smaller closer to the source.

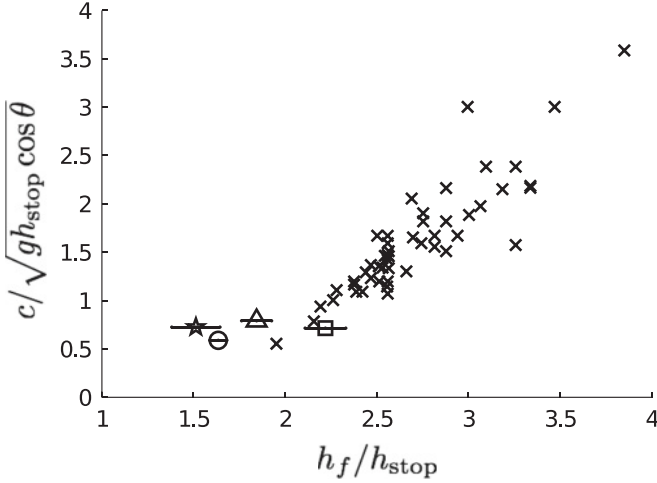


FIG. 24. Dimensionless wave speed plotted against dimensionless thickness of the wave front. Symbols with horizontal error bars represent the mean speed of several avalanches initiated at regular intervals from a point source down a slope with angles \circ , 31.0° ; Δ , 31.5° ; \square , 32.0° ; and \star 32.5° . Vertical error bars are shorter than the size of the symbols. Crosses represent avalanches initiated at irregular intervals from a line source on slopes ranging between 32° and 41° , reproduced from Fig. 2(b) of Börzsönyi *et al.* [37].

IV. DISCUSSION

We propose a simple model of steady flow that incorporates all our observations and focus, in particular, on the relevant issue of what selects the width of the flow. In the central region of the bulk flow, any lateral variation in the layer thickness would be reduced by a cross-stream flow driven by an induced pressure gradient ($\rho gh \cos \theta \nabla h$). Given that the long-time steady flow must be in lateral force balance, and that the central region is yielded and behaves like a fluid, the layer thickness becomes flat over time sufficiently far downstream, as shown for $|y| < 20$ mm in Fig. 11. The layer thickness is governed by the details at the margins, which are independent of the flow width for sufficiently wide flows (Fig. 16). The central region of wide flows has the same constant height h , depth-averaged velocity U , and density ρ , independent of the flow rate Q , in agreement with Fig. 14. An increase in the flow rate results predominantly in an increase in the flow width described by

$$Q = (w - w_0)q, \quad (4)$$

where $q = \rho h U$ is the mass flow rate per unit cross-stream width and w_0 can be interpreted as a correction in the flow width due to the margins. The flow width increases linearly with the mass flow rate Q because w_0 and q depend on the properties of the granular material and the inclined plane but not on Q . The agreement of this model with our experiments is shown by the linear relationships in Fig. 13.

The model of Deboeuf *et al.* [32] has a constant aspect ratio $\gamma = h/w$ independent of the mass flow rate, which does not agree with our experimental results. The assumption of a constant aspect ratio and a scaling analysis of the flow rule (1) imply that w scales like either $Q^{2/5}$ or $Q^{2/7}$ for small

or large Q , respectively. This is inconsistent with the linear relationship between w and Q (Fig. 13). In addition, the model of Deboeuf *et al.* [32] predicts the flow thickness to increase arbitrarily as the flow rate is increased. This could not be in a steady state because a lateral flow would be driven by the much greater hydrostatic pressure under the middle of the flow.

The central region of steady flows has constant thickness and is bounded by regions of constant width, where the thickness and the surface velocity decrease considerably toward the margins (Fig. 16). The height gradient and the strong shear across the flow at the margins are consistent with the second normal stress difference $\sigma_{yy} - \sigma_{zz}$ being negative [38], where σ is the stress tensor. The mechanism responsible for balancing the pressure gradient across the flow could be attributed to flow shear as in viscoelastic fluids, although we have no evidence of this. Note that this mechanism could explain the height gradient at the margins but would not apply to the bulk region where there is little shear in the cross-stream direction. A closer inspection is needed to fully understand the structure of the margin and its stability. We speculate that shallow flows of glass beads are unstable because they are subcritical, meaning that disturbances move faster than the beads on the surface and, hence, can propagate upstream [34]. In contrast, sand flows reported here are supercritical, suggesting that any perturbation of the flow margins decays by the arrival of fresh sand.

In order to estimate the minimum flow rate required for steady flow, we present the following scaling analysis. When the flow rate is far above this minimum, a steady flow develops with thickness h much smaller than the width w of the flow down the inclined plane. The flow is sheared predominantly across its thickness and remains steady down the slope. At larger flow rates, the thickness h remains comparable by order of magnitude to h_{stop} , which is written as $h \sim h_{\text{stop}}$. The dominant length scale of the system is h_{stop} . The other physical quantities with dimensional units are gravity g and the mass flow rate Q , which primarily change the width of the flow only. It follows by dimensional analysis that a suitable scale for the downstream velocity is given by

$$u \sim \sqrt{gh_{\text{stop}}}, \quad (5)$$

which is consistent with Eq. (1). By mass conservation, the mass flow rate,

$$Q \sim \rho u w h_{\text{stop}}, \quad (6)$$

where $\rho \approx 1.5 \text{ kg/m}^3$ is the density of sand. The condition for steady flow is $w \gg h_{\text{stop}}$, which is equivalent to $Q \gg Q_c$, where

$$Q_c \sim \rho g^{1/2} h_{\text{stop}}^{5/2} \quad (7)$$

is obtained by combining Eqs. (5) and (6). Below this critical flow rate, it is not possible to sustain a steady flow with comparable width and thickness. Such a flow would be resisted by lateral stresses and would eventually stop. Instead, avalanches are triggered when a sufficient mass of grains accumulates near the source. Figure 20 shows that Eq. (7) is consistent with experiments.

A feature of the avalanches triggered at regular intervals, which remains to be understood, is that the dimensionless

wave speed is constant on different slopes. Unlike avalanches triggered intermittently from a line source, the avalanches triggered at regular intervals from a point source vary in dimensionless thickness but not in dimensional speed as the slope angle θ changes. The maximal thickness attained near the front of the wave is $h_f = \gamma h_{\text{stop}}$, where γ ranges from 1.4 to 2.4 and depends on θ as shown in Fig. 24. This provides further evidence that a relation, such as Eq. (1), which assumes that the flow speed u and depth h depend on θ only implicitly through h_{stop} , does not hold for the shallow flow of avalanches. The function $\gamma(\theta)$ is not monotonic and is not well understood. Another feature of the avalanches is that they travel steadily like three-dimensional solitons, retaining their shape and size. Dispersive effects due to down-slope variations in thickness may be countered by nonlinear effects due to wave steepening. Cross-slope gradients in the pressure induced by cross-slope variations in thickness of an avalanche flowing down an open slope may be countered by a similar mechanism at the margins of steady flow confined by levees, which would prevent the avalanche from spreading laterally. Some lateral force must counter the pressure gradient induced by the height gradient for an avalanche to retain its shape with more depth in the middle than the edges. The avalanches are not guided by any lateral levees because the erodible layer between successive avalanches is completely flat.

Further insight into the experimental observations could be gained by the development of a mathematical model of avalanches, but this is far from straightforward. One possible approach is to move into the reference frame of an avalanche and to consider the flowing region using a depth-averaged model of shallow granular flow, conserving mass and momentum down the slope [39]. This simplified approach neglects lateral variations and the vertical structure of the avalanche. These features may play an important role particularly near the interface between the flowing and static regions. It is beyond the scope of the present paper to study the exchange of mass across the interface due to erosion and deposition of grains. A better understanding of these processes would be helpful for developing a model, which would predict and would explain the dynamics of avalanches observed in the experiments.

ACKNOWLEDGMENTS

The experimental apparatus was constructed by John Milton, David Page-Croft, Trevor Parkin, and Neil Price. Nicolas Taberlet was involved at an early stage in this project. D.T. is funded by the Gates Cambridge Trust, J.N.M. is funded by the the Engineering and Physical Sciences Council (EPSRC), and H.E.H. is partially supported by the Royal Society.

-
- [1] T. R. H. Davies, *Acta Mech.* **63**, 161 (1986).
 - [2] E. J. Hopfinger, *Annu. Rev. Fluid Mech.* **15**, 47 (1983).
 - [3] X. Cui, J. Gray, and T. Jóhannesson, *J. Geophys. Res.* **112**, F04012 (2007).
 - [4] K. M. Hákonardóttir, A. J. Hogg, J. Batey, and A. W. Woods, *Geophys. Res. Lett.* **30**, 2191 (2003).
 - [5] GDR MiDi, *Eur. Phys. J. E* **14**, 341 (2004).
 - [6] Y. Forterre and O. Pouliquen, *Annu. Rev. Fluid Mech.* **40**, 1 (2008).
 - [7] E. Lajeunesse, A. Mangeney-Castelnau, and J. P. Vilotte, *Phys. Fluids* **16**, 2371 (2004).
 - [8] G. Lube, H. E. Huppert, R. S. J. Sparks, and M. A. Hallworth, *J. Fluid Mech.* **508**, 175 (2004).
 - [9] S. B. Savage and K. Hutter, *Acta Mech.* **86**, 201 (1991).
 - [10] J. Gray, M. Wieland, and K. Hutter, *Proc. R. Soc. London, Ser. A* **455**, 1841 (1999).
 - [11] T. R. Davies and M. J. Mcsaveney, *Can. Geotech. J.* **36**, 313 (1999).
 - [12] A. Daerr, *Phys. Fluids* **13**, 2115 (2001).
 - [13] G. Félix and N. Thomas, *Earth Planet. Sci. Lett.* **221**, 197 (2004).
 - [14] P. A. Lemieux and D. J. Durian, *Phys. Rev. Lett.* **85**, 4273 (2000).
 - [15] M. Tischer, M. I. Bursik, and E. B. Pitman, *J. Sediment. Res.* **71**, 355 (2001).
 - [16] Y. Forterre and O. Pouliquen, *J. Fluid Mech.* **486**, 21 (2003).
 - [17] S. N. Prasad, D. Pal, and M. J. M. Römkens, *J. Fluid Mech.* **413**, 89 (2000).
 - [18] F. Malloggi, J. Lanuza, B. Andreotti, and E. Clément, *Europhys. Lett.* **75**, 825 (2006).
 - [19] E. Azanza, F. Chevoir, and P. Moucheront, *J. Fluid Mech.* **400**, 199 (1999).
 - [20] O. Pouliquen, *Phys. Fluids* **11**, 542 (1999).
 - [21] L. E. Silbert, D. Ertaş, G. S. Grest, T. C. Halsey, D. Levine, and S. J. Plimpton, *Phys. Rev. E* **64**, 051302 (2001).
 - [22] T. Börzsönyi and R. E. Ecke, *Phys. Rev. E* **76**, 031301 (2007).
 - [23] P. Jop, Y. Forterre, and O. Pouliquen, *Nature (London)* **441**, 727 (2006).
 - [24] I. Goldhirsch, *Annu. Rev. Fluid Mech.* **35**, 267 (2003).
 - [25] J. T. Jenkins, *Phys. Fluids* **18**, 103307 (2006).
 - [26] J. Rajchenbach, *Phys. Rev. Lett.* **90**, 144302 (2003).
 - [27] I. S. Aranson, L. S. Tsimring, F. Malloggi, and E. Clément, *Phys. Rev. E* **78**, 031303 (2008).
 - [28] O. Pouliquen and Y. Forterre, *Philos. Trans. R. Soc. London, Ser. A* **367**, 5091 (2009).
 - [29] P. Coussot, S. Proust, and C. Ancey, *J. Non-Newtonian Fluid Mech.* **66**, 55 (1996).
 - [30] N. J. Balmforth, R. V. Craster, and R. Sassi, *J. Fluid Mech.* **470**, 1 (2002).
 - [31] R. R. McDonald and R. S. Anderson, *J. Sediment. Res.* **66**, 642 (1996).
 - [32] S. Deboeuf, E. Lajeunesse, O. Dauchot, and B. Andreotti, *Phys. Rev. Lett.* **97**, 158303 (2006).
 - [33] A. Mangeney, F. Bouchut, N. Thomas, J. P. Vilotte, and M. O. Bristeau, *J. Geophys. Res.* **112**, F02017 (2007).
 - [34] T. Börzsönyi, T. C. Halsey, and R. E. Ecke, *Phys. Rev. E* **78**, 011306 (2008).
 - [35] S. B. Dalziel, DigiFlow, DL Research Partners, version 0.7 (2003).
 - [36] T. Börzsönyi and R. E. Ecke, *Phys. Rev. E* **74**, 061301 (2006).
 - [37] T. Börzsönyi, T. C. Halsey, and R. E. Ecke, *Phys. Rev. Lett.* **94**, 208001 (2005).
 - [38] R. I. Tanner, *J. Rheol.* **14**, 483 (1970).
 - [39] S. B. Savage and K. Hutter, *J. Fluid Mech.* **199**, 177 (1989).